mathematics

MDPI

Article

Numerical Coefficient Reconstruction of Time-Depending Integer- and Fractional-Order SIR Models for Economic Analysis of COVID-19

Slavi Georgiev [1,2,*,†] and Lubin Vulkov [2,†]

[1] Department of Informational Modeling, Institute of Mathematics and Informatics, Bulgarian Academy of Sciences, 1113 Sofia, Bulgaria
[2] Department of Applied Mathematics and Statistics, Faculty of Natural Sciences and Education, University of Ruse, 7004 Ruse, Bulgaria
* Correspondence: sggeorgiev@uni-ruse.bg or sggeorgiev@math.bas.bg; Tel.: +359-82-888-725
† Current address: Department of Applied Mathematics and Statistics, Faculty of Natural Sciences and Education, University of Ruse, 8 Studentska Str., 7004 Ruse, Bulgaria.

Abstract: In the present work, a fractional temporal SIR model is considered. The total population is divided into three compartments—susceptible, infected and removed individuals. It generalizes the classical SIR model and consists of three coupled time-fractional ordinary differential equations (ODEs). The fractional derivative is introduced to account for the subdiffusion process of confirmed, cured and deceased people dynamics. Although relatively basic, the model is robust and captures the real dynamics, helped by the memory property of the fractional system. In the paper, the issue of an adequate model reconstruction is addressed, and a coefficient identification inverse problem is solved; in particular, the transition and recovering rates, varying in time, are recovered. A least-squares cost functional is minimized for solving the problem. The time-dependent parameters are reconstructed with an iterative predictor–corrector algorithm. Its application is demonstrated via tests with synthetic and real data. What is more, an approach for economic impact assessment is proposed.

Keywords: COVID-19 outbreak; SIR modeling; basic reproduction number; Caputo derivative; economic impact

MSC: 34A08; 34A55; 65L09; 92D25; 92D30

Citation: Georgiev, S.; Vulkov, L. Numerical Coefficient Reconstruction of Time-Depending Integer- and Fractional-Order SIR Models for Economic Analysis of COVID-19. *Mathematics* **2022**, *10*, 4247. https://doi.org/10.3390/math10224247

Academic Editor: Ioannis G. Stratis

Received: 14 October 2022
Accepted: 9 November 2022
Published: 13 November 2022

1. Introduction

COVID-19 is an infectious disease caused by a new virus called Severe Acute Respiratory Syndrome Coronavirus 2 (SARS-CoV-2), which emerged in Wuhan, China in December 2019. The subsequent epidemic outbreak has affected the human routine until now, and the situation is not going to change in the near future.

The COVID-19 pandemic has caused widespread damage globally, in terms of human lives and international economic weakening. As a new highly contagious disease, governments have taken unprecedented measures to slow down the spread of the virus, including quarantines, curfews, lockdowns and national and international travel suspensions.

The spread of the COVID-19 infectious disease involves not only diseased-related factors, such as the infectious agent, mode of transmission, latent period, infectious period, susceptibility and resistance, but also social, cultural and demographic factors and, what is most important, *economics* and *finance*.

Mathematical modeling is an essential tool for understanding the spread of the disease. Such models raise awareness about the transmission dynamics of a broad class of infectious diseases. Disease transmission may be modeled as a compartment model, in which the population in consideration is divided into compartments under assumptions about the

nature and time rate of transfer from one compartment to another [1]. Usually, they are composed by a system of ordinary differential equations (ODEs) in time, which model the rate of change, or inbound and outbound flow in every compartment.

We adopted the most fundamental compartment model, constituted by three compartments, namely the susceptible (S), infected (I) and removed (R) individuals. This SIR model is proposed by [2], and subsequently has undergone enormous investigation and further development [3]. The nonlocal fractional operators find broad application in the study of biological phenomena [4]. Being far from exhaustive, we only mention a couple of studies. A SIR model, taking account of vaccinations and waning immunity is considered in [5]. A fractional SIR model with constant vaccination rate is explored in [6], and a similar model is proposed and analyzed in [7]. A nonlinear fractional SIR model with special types of functional response and treatment rate is studied in [8]. Inverse problems [9] concerning constant parameter estimation is studied in [10], and time-dependent coefficient recoveries as piecewise constant functions of time in a SIR model are examined in [11,12]. The recovery of pandemic dynamics and their economic impact in view of constant parameters by means of the adjoint equation optimization approach for integer- and fractional-order SEIR models is performed in [13,14]. We talk about the SIR model in greater detail in the next section.

The question of how to minimize the economic damage of a lockdown while still containing infectious is studied in [15]. The authors used the model (1) in the case of $\beta = \beta(t)$ and $\gamma = \text{const} > 0$. When and how much to impose lockdown so that the damage to the economy is minimized? The crucial ingredient in our study is the use of a new time variable.

How effective are the social distancing approaches? We use time-dependent coefficient Susceptible-Infected-Removed (SIR) models that track two time series:

(i) The transition rate β at time t;
(ii) The recovering rate γ at time t.

Such an approach is not only more adaptive than traditional static SIR models but also more robust than direct estimation methods.

The next section, as we mentioned, is devoted to the formulation of the integer- and fractional-order models, as well as the definition of the direct and inverse problems of epidemic modeling. Section 3 recalls some results from the fractional calculus needed henceforward. In Section 4, the solution to the direct problem is briefly discussed, while in Section 5, the algorithm for solving the inverse problems is presented in detail. Section 6 is dedicated to the framework for estimating the economic impact of the pandemic, and in Section 7, the proposed algorithm is tested with synthetic and real data. The paper is concluded in Section 8.

2. Problems Formulation

In this section, starting from the classical SIR models, we introduce the Caputo fractional operator SIR model. For the last one, we formulate direct and inverse point observation problems.

2.1. The Classical SIR Model

The study of infectious disease proliferation is a well-established field and has given rise to the area of science called *mathematical epidemiology*. Mathematical epidemiology proposes models that help the understanding of epidemics and outlining policies to control infectious diseases. These models have been extensively used in biological, ecological and chemical applications [16]. They allow for understanding the processes involved and for predicting the dynamics of the epidemic.

The propagation of an infectious disease in a population that is assumed to be constant-sized over the period of the epidemic can be formulated by the first-order ODE system

$$\begin{aligned} \mathrm{D}_t S(t) &= -\beta(t)S(t)I(t), \\ \mathrm{D}_t I(t) &= \beta(t)S(t)I(t) - \gamma(t)I(t), \\ \mathrm{D}_t R(t) &= \gamma(t)I(t) \end{aligned} \tag{1}$$

with initial conditions

$$S(t_0) = S_0,\ I(t_0) = I_0,\ R(t_0) = R_0,$$

where at time $t \geq t_0$, $S(t)$ is the level of the susceptible individuals, $I(t)$ is the level of infected people who are able to spread the disease by contact with susceptible ones and $R(t)$ is the level of isolated individuals who cannot get or transmit the disease for various reasons. Additionally, $0 \leq S_0, I_0, R_0 \leq 1$. Moreover, $\beta(t) > 0$ is the rate of infection, and $\gamma(t) > 0$ is the rate at which the current infectious population is isolated.

2.2. A Fractional SIR Model

The SIR model is undoubtedly the most famous mathematical model for the propagation of an infectious disease. In many cases, however, the classical derivative is not able to precisely describe the complex phenomena of the disease. Aiming at the latter, many researchers try to model, as well as to analyze, the dynamic behavior of the process by means of fractional calculus. The fractional-order extension of the model was first studied in [17], where the authors replace the first-order derivative in (1) by Caputo's fractional derivative of order $0 < \alpha \leq 1$ [18].

The use of $\alpha < 1$ just has the effect of transforming (1) into a model with memory. In general, the epidemic integer model (1) does not carry any information about the memory and learning mechanism of the population that affects the spread of disease; see e.g., [19].

Without loss of generality, we assume that the process starts at time $t_0 = 0$. Then, we consider the following fractional system of ODEs

$$\mathrm{D}_0^\alpha S(t) = -\beta^\alpha(t)S(t)I(t), \tag{2a}$$

$$\mathrm{D}_0^\alpha I(t) = \beta^\alpha(t)S(t)I(t) - \gamma^\alpha(t)I(t), \tag{2b}$$

$$\mathrm{D}_0^\alpha R(t) = \gamma^\alpha(t)I(t). \tag{2c}$$

with initial conditions

$$S(0) = S_0 \geq 0,\ I(0) = I_0 \geq 0,\ R(0) = R_0 \geq 0. \tag{3}$$

Here, D_0^α is the left Caputo fractional derivative operator of order $0 < \alpha \leq 1$; see the next section.

If the unit in the model (1) is days^{-1}, the Caputo operator D_0^α is in unit days$^{-\alpha}$. In order to keep the units the same in both hand sides of (2), we raise the coefficients to the power of α.

There exist other models considering additional events and features, such as birth and death rates (non-constant population), vaccine effect, reinfection, latent period and so on; see, e.g., [5,11]. In this work, we use the fractional SIR model, but the integer ($\alpha = 1$) case is also independently studied.

2.3. The Basic Reproduction Number

The *basic reproduction number* $\mathcal{R}_0$ is a very significant quantity in the theory of infectious disease modeling. Roughly speaking, it measures how contagious a particular disease is [20]. A substantial finding in mathematical epidemiology is the abrupt change in the behavior of the epidemic, based on whether the basic reproduction number is bigger than one or less than one. This is an illustration of the threshold behavior phenomenon [21].

If the vital dynamics are not incorporated in the model, as it is the case with (1), the basic reproduction number is calculated easily. For a SIR model, it is

$$\mathcal{R}_0 = \frac{\beta(t)}{\gamma(t)}. \tag{4}$$

For the fractional-order derivative model (2), it follows:

$$\mathcal{R}_0 = \frac{\beta^\alpha(t)}{\gamma^\alpha(t)}. \tag{5}$$

More formally, the value of the basic reproduction number $\mathcal{R}_0$ represents the average number of secondary infections caused by a single infective over his/her period of infectiousness, introduced in a wholly susceptible population. Essentially, if the value of the basic reproduction number is less than one ($\mathcal{R}_0 < 1$), then the epidemic is in its dusk. On the contrary, if $\mathcal{R}_0 > 1$, then the infection continues to spread around the susceptible population [22].

2.4. The Direct and Inverse Problems

The functions $S(t)$, $I(t)$ and $R(t)$ satisfy the *direct problem*, if the coefficients β and γ are known. In practice, the parameters β and γ are not known (since they cannot be measured directly), and they have to be recovered. After their «fair» values are found, the model could be used for subsequent analysis.

The main issue is how to find the values $\boldsymbol{p} \equiv \{\beta, \gamma\}$ for a given infection, for instance, COVID-19, if the levels of the susceptible and infected population are known at certain times

$$\begin{array}{ll} S(t_k;\boldsymbol{p}) = X_k, & k = 1, \ldots, K_S, \\ I(t_k;\boldsymbol{p}) = Y_k, & k = 1, \ldots, K_I. \end{array} \tag{6}$$

The estimation of the parameter $\boldsymbol{p}$ is referred to as an *inverse modeling problem*. It means adjusting the parameter values of a mathematical model to reproduce measured data.

The measurements (6) are called *point observations*, and the values of the parameters are found usually by minimization of a functional of type

$$J = J(\boldsymbol{p}) = \sum_{k=1}^{K_S} \left[S(t_k;\boldsymbol{p}(t)) - X_k\right]^2 + \sum_{k=1}^{K_I} \left[I(t_k;\boldsymbol{p}(t)) - Y_k\right]^2, \quad t \in [t_0, t_K].$$

3. Auxiliary Results on Fractional Calculus

In this section, we provide some notations, fractional mean value formulae and formulae for integration by parts. Moreover, we establish a theorem that provides a simple criterion on the right-hand side of a fractional ODE system that tells us whether the system is positive.

Hereinafter, Γ denotes the Gamma function $\Gamma(s) := \int_0^\infty \eta^{s-1} e^{-\eta} \mathrm{d}\eta$ for $s > 0$. We recall that $\Gamma(s+1) = s\Gamma(s)$ for all $s > 0$ and for any positive integer n, $\Gamma(n) = (n-1)!$ is true.

For arbitrary function $\nu \in \mathcal{AC}[0, T]$, i.e., ν is absolutely continuous on $[0, T]$, the left (forward) Riemann–Liouville integral for $\alpha \in [0, 1]$ is defined as [23]:

$$\left(J_{0^+}^\alpha \nu\right)(t) := \begin{cases} \nu(t), & \alpha = 0, \\ \dfrac{1}{\Gamma(\alpha)} \displaystyle\int_0^t \frac{\nu(s)}{(t-s)^{1-\alpha}} \mathrm{d}s, & 0 < \alpha \leq 1, \end{cases} \quad t \in [0, T).$$

The left (forward) Caputo derivative is written as:

$${}^{\mathfrak{C}}\mathrm{D}_0^\alpha \nu(t) = \left(J_{0^+}^{1-\alpha} \frac{\mathrm{d}\nu}{\mathrm{d}t}\right)(t) = \frac{1}{\Gamma(1-\alpha)} \int_0^t \frac{1}{(t-s)^\alpha} \frac{\mathrm{d}\nu}{\mathrm{d}t} \mathrm{d}s.$$

We define the left (forward) Riemann–Liouville derivative as follows:

$$ {}^{\mathfrak{R}}\mathrm{D}_0^{\alpha}\nu(t) = \frac{\mathrm{d}}{\mathrm{d}t}\left(J_{0^+}^{1-\alpha}\nu\right)(t) = \frac{1}{\Gamma(1-\alpha)}\frac{\mathrm{d}}{\mathrm{d}t}\int_0^t \frac{\nu(s)}{(t-s)^{\alpha}}\mathrm{d}s. $$

The right (backward) fractional integral could be defined as

$$ \left(J_{T^-}^{\alpha}\nu\right)(t) := \begin{cases} \nu(t), & \alpha = 0, \\ \dfrac{1}{\Gamma(\alpha)}\displaystyle\int_t^T \frac{\nu(s)}{(s-t)^{1-\alpha}}\mathrm{d}s, & 0 < \alpha \le 1, \end{cases} \quad t \in (0,T], $$

hence, we define the right (backward) Caputo and Riemann–Liouville derivatives as

$$ {}^{\mathfrak{C}}\mathrm{D}_T^{\alpha}\nu(t) = -\left(J_{T^-}^{1-\alpha}\frac{\mathrm{d}\nu}{\mathrm{d}t}\right)(t) = -\frac{1}{\Gamma(1-\alpha)}\int_t^T \frac{1}{(s-t)^{\alpha}}\frac{\mathrm{d}\nu}{\mathrm{d}t}(s)\mathrm{d}s, $$

$$ {}^{\mathfrak{R}}\mathrm{D}_T^{\alpha}\nu(t) = -\frac{\mathrm{d}}{\mathrm{d}t}\left(J_{T^-}^{1-\alpha}\nu\right)(t) = -\frac{1}{\Gamma(1-\alpha)}\frac{\mathrm{d}}{\mathrm{d}t}\int_t^T \frac{\nu(s)}{(s-t)^{\alpha}}\mathrm{d}s. $$

The relationship between the Caputo and Riemann–Liouville forward and backward derivatives is written as

$$ {}^{\mathfrak{C}}\mathrm{D}_0^{\alpha}f(t) = {}^{\mathfrak{R}}\mathrm{D}_0^{\alpha}f(t) - \frac{f(0)}{\Gamma(1-\alpha)}t^{-\alpha},\ t \in (0,T], $$

$$ {}^{\mathfrak{C}}\mathrm{D}_T^{\alpha}f(t) = {}^{\mathfrak{R}}\mathrm{D}_T^{\alpha}f(t) - \frac{f(T)}{\Gamma(1-\alpha)}(T-t)^{-\alpha},\ t \in (0,T]. $$

We state here the following version of integration by parts [23].

Lemma 1. *Let $\nu_1(t), \nu_2(t) \in \mathcal{C}^1[0,T]$. Then,*

$$ \int_0^T \left({}^{\mathfrak{C}}\mathrm{D}_0^{\alpha}\nu_1\right)\nu_2\mathrm{d}t + \nu_1(0)\left(J_{T^-}^{1-\alpha}\nu_2\right)(0) = \int_0^T \nu_1\left({}^{\mathfrak{C}}\mathrm{D}_T^{\alpha}\nu_2\right)\mathrm{d}t + \left(J_{T^-}^{1-\alpha}\nu_1\right)(T)\nu_2(T). $$

We also recall the *generalized mean value formula (GMF)* in the following form [23]. Suppose $f(t) \in \mathcal{C}[a,b]$ and $\mathrm{D}_0^{\alpha}f(t) \in \mathcal{C}[a,b]$ for $0 < \alpha \le 1$, then we have

$$ f(t) = f(0) + \frac{1}{\Gamma(\alpha)}\mathrm{D}_0^{\alpha}f(\xi)t^{\alpha} \text{ with } 0 \le \xi \le t,\ \forall t \in [a,b]. $$

It easily follows that if $\mathrm{D}_0^{\alpha}f(t) \ge 0\ \forall t \in (a,b)$, then the function $f(t)$ is nondecreasing for each $t \in [a,b]$, and if $\mathrm{D}_0^{\alpha}f(t) \le 0\ \forall t \in (a,b)$, then the function $f(t)$ is nonincreasing $\forall t \in [a,b]$.

In the following, we write $v \ge 0$ for a vector $v \in \mathbb{R}^m$ if all components are non-negative. Consider a fractional ODE system in $\mathbb{R}^m$ for $t \ge 0$,

$$ \mathrm{D}_t^{\alpha}w(t) = F\big(t, w(t)\big). \tag{7} $$

This system is called *positive* (short for "non-negativity preserving") if

$$ w(0) \ge 0 \ \Rightarrow\ w(t) \ge 0 \quad \forall t > 0. $$

The next assertion generalizes Theorem 7.1 in [24].

Theorem 1. *Suppose that $F(t,v)$ is continuous and satisfies the Lipschitz condition*

$$ \|F(t,\bar{v}) - F(t,v)\| \le L\|\bar{v} - v\|\ \forall (t,\bar{v}) \in \mathbb{C}_0, $$

where $\mathbb{C}_0$ *is the cylinder*

$$\mathbb{C}_0 \equiv \{(t,v) \in \mathbb{R} \times \mathbb{R}^m : 0 \le t \le T, \|v - w(0)\| \le K_0\}.$$

Then, the system (2) *is positive if for any vector* $v \in \mathbb{R}^m$ *and all* $i = 1, \ldots, m$ *and* $t \ge 0$,

$$v \ge 0, v_i = 0 \;\Rightarrow\; F_i(t,v) \ge 0.$$

Proof. The necessity of the above criterion follows immediately by considering the solution (7) $w(t)$ with $w(0) = v$ and small $t > 0$. As for sufficiency, note that the criterion is equivalent to

$$w(t) \ge 0, w_i(t) = 0 \;\Rightarrow\; \mathrm{D}_t^\alpha w_i(t) \ge 0$$

and GMF implies $w_i(t) \ge 0$. This is by itself not enough to prove positivity; we need the Lipschitz condition.

It would be enough to have

$$w(t) \ge 0, w_i(t) = 0 \;\Rightarrow\; \mathrm{D}_t^\alpha w_i(t) \ge \varepsilon > 0,$$

because then it is obvious that $w(t)$ cannot cross the hyperplanes $\mathcal{H}_i = \{w \in \mathbb{R}^m : w_i = 0\}$. This holds for the perturbed ODE system with

$$\tilde{F}_i(t,w) = F_i(t,w) + \varepsilon,\ i = 1, 2, \ldots, m.$$

Using the Lipschitz condition, we can apply a stability argument for fractional ODEs to show that the solution to the unperturbed system with given $w(0)$ could be approximated with any precision by solutions to the perturbed system if we let $\varepsilon \to 0$. □

4. Solution to the Direct Problem

In this section, we discuss some basic properties of the problem (2), (3) and then we describe algorithms to solve numerically the direct problems (1) or (2), (3).

Firstly, let us emphasize that by applying Theorem 3.1. and Remark 3.2. of [25], one could easily obtain the global existence and uniqueness of the solution to problem (2), (3).

4.1. Properties of the Continuous Solution

It is a natural requirement for the models of real-life phenomena, in particular (2), (3), that their solutions must possess some basic qualitative properties of the original (constant coefficient) process. In the present case, such qualitative properties are as follows:

P1 The total size of the population at a given spatial position cannot change in time. It simply follows by adding the three equations in (2) together

$$\mathrm{D}_t^\alpha \big(S(t) + I(t) + R(t)\big) = 0.$$

Hence, a basic property of the Caputo's derivative gives

$$S(t) + I(t) + R(t) = 1 = S_0 + I_0 + R_0.$$

P2 The number of the susceptible, infected and removed members (people) must be non-negative.

In order to prove **P2**, we need the results from Section 3 concerning *positive* fractional ODE systems. Eventually, the property **P2** follows by direct application of Theorem 1 to problem (2), (3).

P3 The number of the susceptible cannot grow and the number of the removed cannot decrease in time. That is, the function $S(t)$ is decreasing while the function $R(t)$ is increasing. If

$$S(0) < \frac{\gamma(t)}{\beta(t)},$$

the number of the infected cannot grow, that is, the function $I(t)$ is decreasing.

4.2. Numerical Solution

In this subsection, we describe how to solve the direct problems (1) and (2). It is important since the direct problems have to be solved a number of times in order to solve the inverse problem. Without loss of generality, we use an equidistant temporal mesh

$$\overline{\omega}_{\triangle t}^{\mathrm{dir}} = \{t_0, t_j = j\triangle t, t_J = T\} \text{ for } j = 1, \ldots, J-1 \tag{8}$$

with constant step size $\triangle t$.

From now on, due to the closedness of the system (1) or (2), we can exclude the equation for $\mathrm{D}R(t)$ and work with the first two equation. If the three compartments exhaust the society, then $R(t) = 1 - S(t) - I(t)$ for every $t \geq t_0$.

The first to consider would be the integer-order model. A standard approach is to apply the Runge–Kutta method. If we write (1) in the form

$$\frac{\mathrm{d}\boldsymbol{R}}{\mathrm{d}t} = \boldsymbol{G}\big(t, \boldsymbol{R}(t)\big),$$

where $\boldsymbol{R} = (S, I)^\top$ and $\boldsymbol{R}_0 = \boldsymbol{R}(t_0)$, then the Algorithm 1 looks like

Algorithm 1 Runge–Kutta method [26]

for $j = 0, \ldots, J-1$ **do**

Let $t := t_j$, $\hat{t} := t_{j+1}$, $\boldsymbol{R} := \boldsymbol{R}(t)$, $\hat{\boldsymbol{R}} := \boldsymbol{R}(\hat{t})$. Then, $\hat{\boldsymbol{R}}$ is calculated as

$$\hat{\boldsymbol{R}} = \boldsymbol{R} + \frac{\triangle t}{6}(\boldsymbol{k}_1 + 2\boldsymbol{k}_2 + 2\boldsymbol{k}_3 + \boldsymbol{k}_4),$$

where

$$\boldsymbol{k}_1 = \boldsymbol{G}(t,\ \boldsymbol{R}), \quad \boldsymbol{k}_2 = \boldsymbol{G}\left(t + \frac{\triangle t}{2},\ \boldsymbol{R} + \frac{\boldsymbol{k}_1}{2}\right),$$
$$\boldsymbol{k}_3 = \boldsymbol{G}\left(t + \frac{\triangle t}{2},\ \boldsymbol{R} + \frac{\boldsymbol{k}_2}{2}\right), \quad \boldsymbol{k}_4 = \boldsymbol{G}(\hat{t},\ \boldsymbol{R} + \boldsymbol{k}_3).$$

end for

For the fractional-order model, we use the same mesh $\overline{\omega}_{\triangle t}^{\mathrm{dir}}$ (8). Here, we apply the generalized Adams–Bashforth–Moulton, or the fractional Adams method. Equation (2) in the form

$${}^{\mathfrak{C}}\mathrm{D}_0^{\alpha}\boldsymbol{R} = \boldsymbol{G}\big(t, \boldsymbol{R}(t)\big)$$

is equivalent to the Volterra integral equation

$$\boldsymbol{R}(t) = \boldsymbol{R}_0 + \frac{1}{\Gamma(\alpha)}\int_0^t \frac{\boldsymbol{G}\big(s, \boldsymbol{R}(s)\big)}{(t-s)^{1-\alpha}}\mathrm{d}s,$$

which is solved by Algorithm 2. It is again a single-step method, requiring only knowledge of the initial condition to commence.

Algorithm 2 Fractional Adams method [27]

for $j = 0, \ldots, J-1$ **do**

Let $t := t_j$, $\hat{t} := t_{j+1}$, $\boldsymbol{R} := \boldsymbol{R}(t)$, $\hat{\boldsymbol{R}} := \boldsymbol{R}(\hat{t})$. Then, $\hat{\boldsymbol{R}}$ is calculated as

$$\hat{\boldsymbol{R}}^{\text{pred}} = \boldsymbol{R}_0 + \frac{1}{\Gamma(\alpha)} \sum_{i=0}^{j} b_{i,j+1} \boldsymbol{G}(t, \boldsymbol{R}),$$
$$\hat{\boldsymbol{R}} = \hat{\boldsymbol{R}}_0 + \frac{1}{\Gamma(\alpha)} \left(\sum_{i=0}^{j} a_{i,j+1} \boldsymbol{G}(t, \boldsymbol{R}) + a_{i+1,j+1} \boldsymbol{G}(\hat{t}, \hat{\boldsymbol{R}}^{\text{pred}}) \right),$$

where

$$a_{i,j+1} = \frac{\triangle t^{\alpha}}{\alpha(\alpha+1)} \begin{cases} j^{\alpha+1} - (j-\alpha)(j+1)^{\alpha}, & i = 0, \\ (j-i+2)^{\alpha+1} - 2(j-i+1)^{\alpha+1} + (j-i)^{\alpha+1}, & 1 \le i \le j, \\ 1, & i = j+1, \end{cases}$$

$$b_{i,j+1} = \frac{\triangle t^{\alpha}}{\alpha} \left((j-i+1)^{\alpha} - (j-i)^{\alpha} \right), \qquad 0 \le i \le j.$$

end for

The presented methods are some of the most widely used but simple approaches. Of course, other more complicated methods, possibly of higher order, could be successfully applied.

5. Numerical Solution to the Inverse Problem

In this section, we reveal the computational algorithm for numerically solving the inverse problems (1) or (2), (3), (6) in detail.

We use different notations for the time instances. The temporal mesh $\overline{\omega}^{\text{inv}}_{\triangle t}$ (9) is displayed in Figure 1.

$$\overline{\omega}^{\text{inv}}_{\triangle t} = \{t_0^* = T_0^*, t_j^* = j\triangle t, t_J^* = T_K^*\} \text{ for } j = 1, \ldots, J-1. \tag{9}$$

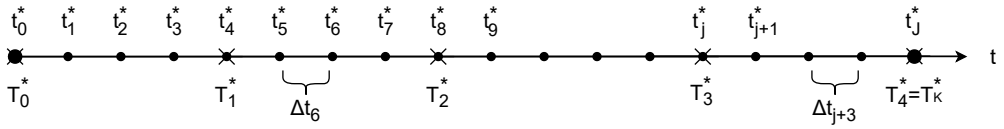

Figure 1. The mesh $\overline{\omega}^{\text{inv}}_{\triangle t}$ for $K = 4$.

The points t_j^* denote every time instance where the values of the system functions S and I are known. In practice, their levels (although not in this form) are reported every day. On the other hand, for the ease of calculation, it is appropriate that the observation points coincide with nodes after discretization, but we are free to choose an arbitrary fine mesh since the algorithm does not require the presence of measurement in every node (the observation points are a subset of the discrete time nodes).

We propose an algorithm that recovers the unknown dynamics parameters as piecewise linear functions of time. To achieve this, the functions are reconstructed in a step-by-step manner. If we iterate over the measurements t_j^*, we would arrive at nicely waved functions but at very high cost. On the other extreme case, if we use as little as one or two measurements, then very fast we would obtain just a straight line. So, we must perform a trade-off between fit and speed.

In order to achieve it, we introduce the so-called 'main' observations, denoted with T_k^* (9) (Figure 1). In practice, it is best for them to be distributed in such a way that the space between adjacent main points to be $1 \div 2$ weeks. For simplicity, in the exposition henceforward, we assume constant time step $\triangle t$ and $K_S = K_I = K$.

The indices $k = 1, \ldots, K$ in the observation definition (6) match the indices $j = 1, \ldots, J$ in the following way:

$$T_k^* \equiv t_{m_k}^* \text{ for } k = 1, \ldots, K.$$

As we discussed earlier, the unknown parameters $\beta(t)$ and $\gamma(t)$ are recovered step by step. For iterator, we use k, since on iteration k, we use the information available up to T_k^*. The computational algorithm readily follows:

Step 1.1. Minimize the cost functional

$$J_1(\beta, \gamma) = \sum_{k=m_0+1}^{m_1} \left[S\left(t_k; \beta(t), \gamma(t)\right) - X_k\right]^2 + \left[I\left(t_k; \beta(t), \gamma(t)\right) - Y_k\right]^2, \; t \in [T_0^*, T_1^*].$$

Now, (β_1, γ_1) is the minimum of J_1. Here, the parameter functions are assumed to be constant in $[T_0^*, T_1^*]$ due to the nonuniqueness of the local minimum if using a linear function. The suggested algorithm is of predictor–corrector type, so the final coefficient values in $[T_0^*, T_1^*]$ would be linear functions of time. This would be achieved during the next step.

Step 1.2. The current values of the parameters are

$$\begin{aligned} \beta^{(1)}(t) &= \beta_1 \quad \text{for } t \in [T_0^*, T_1^*], \\ \gamma^{(1)}(t) &= \gamma_1 \quad \text{for } t \in [T_0^*, T_1^*]. \end{aligned}$$

Step 2.1. Minimize the cost functional

$$J_2(\beta, \gamma) = \sum_{k=m_0+1}^{m_2} \left[S\left(t_k; \beta(t), \gamma(t)\right) - X_k\right]^2 + \left[I\left(t_k; \beta(t), \gamma(t)\right) - Y_k\right]^2, \; t \in [T_0^*, T_2^*].$$

If the minimum of J_2 is (β_2, γ_2), then the parameters are assumed to be linear in $[T_0^*, T_2^*]$, and these linear functions are constructed according to the rules: $\beta^{(2)}(T_{1/2}) = \beta_1$ and $\beta^{(2)}(T_2^*) = \beta_2$, where we denote $T_{j+1/2} = (T_j^* + T_{j+1}^*)/2$ for $j = 0, \ldots, J-1$. The same rules apply for $\gamma^{(2)}$. More rigorously, they are computed via

$$\begin{aligned} a_2^\beta &= \frac{\beta_2 - \beta_1}{T_2^* - T_{1/2}}, \qquad a_2^\gamma = \frac{\gamma_2 - \gamma_1}{T_2^* - T_{1/2}}, \\ b_2^\beta &= -T_2^* a_2^\beta + \beta_2, \quad b_2^\gamma = -T_2^* a_2^\gamma + \gamma_2. \end{aligned}$$

We again recall that the correction part on this step affects the whole interval $[T_0^*, T_1^*]$ of the first step.

Step 2.2. The recovered parameters are

$$\begin{aligned} \beta^{(2)}(t) &= a_2^\beta t + b_2^\beta \quad \text{for } t \in [T_0^*, T_2^*], \\ \gamma^{(2)}(t) &= a_2^\gamma t + b_2^\gamma \quad \text{for } t \in [T_0^*, T_2^*]. \end{aligned}$$

The following step is iteratively repeated from $k = 3$ to $k = K$.

Step k.1. Minimize the cost functional

$$J_k(\beta, \gamma) = \sum_{k=m_{k-3/2}}^{m_k} \left[S\left(t_k; \beta(t), \gamma(t)\right) - X_k\right]^2 + \left[I\left(t_k; \beta(t), \gamma(t)\right) - Y_k\right]^2, \; t \in [T_{k-3/2}, T_k^*],$$

where $m_{k-3/2}$ is such that $t_{m_{k-3/2}}^*$ is the closest observation point to $T_{k-3/2}$.

Let again the minimum of J_k be (β_k, γ_k), then the coefficient values in $[T_{k-3/2}, T_k^*]$ again are assumed to be linear functions. They satisfy $\beta^{(k)}(T_{k-3/2}) = \beta^{(k-1)}(T_{k-3/2})$ and $\beta^{(k)}(T_k^*) = \beta_k$, which is also true for $\gamma^{(k)}$:

$$a_k^\beta = \frac{\beta_k - \beta^{(k-1)}(T_{k-3/2})}{T_k^* - T_{k-3/2}}, \quad a_k^\gamma = \frac{\gamma_k - \gamma^{(k-1)}(T_{k-3/2})}{T_k^* - T_{k-3/2}},$$
$$b_k^\beta = -T_k^* a_k^\beta + \beta_k, \qquad b_k^\gamma = -T_k^* a_k^\gamma + \gamma_k.$$

In this case, the correction part of the step affects the latest half-step $[T_{k-3/2}, T_{k-1}^*]$.

Step k.2. The identified parameters are

$$\beta^{(k)}(t) = a_k^\beta t + b_k^\beta \quad \text{for } t \in [T_{k-3/2}, T_k^*],$$
$$\gamma^{(k)}(t) = a_k^\gamma t + b_k^\gamma \quad \text{for } t \in [T_{k-3/2}, T_k^*].$$

Eventually, the output of the algorithm is constructed as follows:

Step K + 1. Compute

$$\beta(t) = \begin{cases} \beta^{(2)}(t) & \text{for } t \in [T_0^*, T_{3/2}], \\ \beta^{(k)}(t) & \text{for } t \in [T_{k-3/2}, T_{k-1/2}] \text{ for } 2 < k < K, \\ \beta^{(K)}(t) & \text{for } t \in [T_{K-3/2}, T_K^*], \end{cases}$$
$$\gamma(t) = \begin{cases} \gamma^{(2)}(t) & \text{for } t \in [T_0^*, T_{3/2}], \\ \gamma^{(k)}(t) & \text{for } t \in [T_{k-3/2}, T_{k-1/2}] \text{ for } 2 < k < K, \\ \gamma^{(K)}(t) & \text{for } t \in [T_{K-3/2}, T_K^*]. \end{cases}$$

The parameters are reconstructed as piecewise linear functions of time for $t \in [T_0^*, T_K^*]$.

In every step, the nonlinear estimators are short vectors, the length of which depends on the number of recovered parameters (two in our case). This makes the algorithm fast to converge. Its ability to work with real data is demonstrated further.

6. Economic Loss from Social Distancing

To estimate the economic impact of the pandemic, we adopt the approach proposed in [28]. The losses are twofold. The first element delineates losses due to infections, while the second one accounts for losses related to the restrictions in the contacts volume. The original model follows (10):

$$\mathrm{L} = a \int_\tau^{\tau^*} I(t)\mathrm{d}t + b(\beta_0 - \beta_1)(\tau^* - \tau), \tag{10}$$

where $0 < \tau < \tau^*$ and a and b are non-negative constants. It is assumed that in the period $[0, \tau)$ no measures are applied, while in $[\tau, \tau^*]$ strict measures are imposed. The second component of (10) assumes also that the transmission rate β is a simple piecewise constant function of time: $\beta(t) = \beta_0 \mathbb{1}_{\{t<\tau\}} + \beta_1 \mathbb{1}_{\{\tau \le t < \tau^*\}}$, where $\beta_0 > \beta_1$; see [28].

The first element in L is simply explained, as the infected individuals may need hospitalization or intensive care and might not be able to work.

The second component in L accounts for the fact that, when contact number is reduced by the imposed social distancing measures, the corresponding reduction in economic product per unit of time is to some extent proportional to the reduction in the level of contacts. As the infection is transmitted by mass action (contacts between infectious and susceptible), β can be considered as proportional to the average number of contacts per person. Thus, the reduction in the number of contacts during $[\tau, \tau^*]$ is proportional to $\beta_0 - \beta_1$.

To make the concept work with arbitrary function of time, we have to generalize the concept of contact level decreasing. It is the negative derivative of the transmission rate $\beta(t)$, or $\mathrm{D}\beta(t) < 0$. The greater the drop in β, the larger the economic losses are.

So, basically, we have to integrate the transmission coefficient in the intervals where the derivative is negative:

$$\mathrm{L}_0^T = N\left(a\int_0^T I(t)\mathrm{d}t + b\int_0^T -\beta'(t)\mathbb{1}_{\{\beta'(t)<0\}}\mathrm{d}t\right), \tag{11}$$

where N is the total population size [29].

7. Computational Experiments

This section is devoted to ample numerical simulations, which demonstrate the properties of the proposed algorithm. In the following subsections, computational tests for both integer- (Section 7.1) and fractional-order (Section 7.2) models with synthetic and real data are performed. The section is concluded with a real-world data example (Section 7.3).

The quasi-real experiments are conducted as follows. Firstly, we make up values for $\beta(t)$ and $\gamma(t)$ and solve the direct problem (1) or (2). Furthermore, we derive the synthetic measurements (6) from the solution. On the next stage, we supply the procedure for solving the inverse problem with these measurements. The algorithm result is composed by the implied $\beta(t)$ and $\gamma(t)$, which we could compare with the true ones, those which were used to solve the direct problem.

However, in a real setting, the main problem is that we do not know the true $\beta(t)$ and $\gamma(t)$. We take the measurements from reality and solve the inverse problem. In order to assess the algorithm performance, we need another indicator. The name «goodness-of-fit» suggests that we could solve the direct problem with the *implied* parameters and then compare the values of the real data $S(t)$ and $I(t)$ with the "implied" functions, i.e., those obtained by Algorithm 1 or Algorithm 2 fed with the implied coefficients.

7.1. Integer-Order Derivative Model

We begin the tests with the integer-order model (1). The discretization is conducted according to Algorithm 1. The nodes in mesh $\overline{\omega}^{\mathrm{inv}}_{\triangle t}$ are equidistantly distributed with constant step size 0.1, and the space between observations is $\triangle t = 2$, i.e., data are available every two days. To cope with the nonlinear nature of the coefficients, we assume the main observations are also placed on every second day, i.e., they overlap.

We set the initial condition $S_0 = 0.9$, $I_0 = 0.09$, $[t_0, T] \equiv [0, 20]$, and firstly we test with the nonlinear functions

$$\beta(t) = \frac{3}{5}e^{-\frac{t}{T}} \text{ and } \gamma(t) = \frac{2}{5} + \frac{1}{20}\left(\frac{t}{T}\right)^2. \tag{12}$$

The results are plotted on Figures 2 and 3.

A good fit is observed, and therefore the real and implied system functions match as well. To quantify the latter, we introduce the residual norm

$$R\big(\beta(t),\gamma(t)\big) = \big\|S\big(\beta(t),\gamma(t)\big) - X\big\|_2 + \big\|I\big(\beta(t),\gamma(t)\big) - Y\big\|_2. \tag{13}$$

For the first case, $R\big(\beta(t),\gamma(t)\big) = 0.0031$.

To test with more volatile coefficients, we add oscillation terms such that the parameter functions now are

$$\beta(t) = \frac{3}{5}e^{-\frac{t}{T}} + \frac{1}{10}\sin\frac{4\pi t}{T} \text{ and } \gamma(t) = \frac{2}{5} + \frac{1}{20}\left(\frac{t}{T}\right)^2 + \frac{1}{10}\cos\frac{4\pi t}{T}. \tag{14}$$

The results are displayed on Figures 4 and 5.

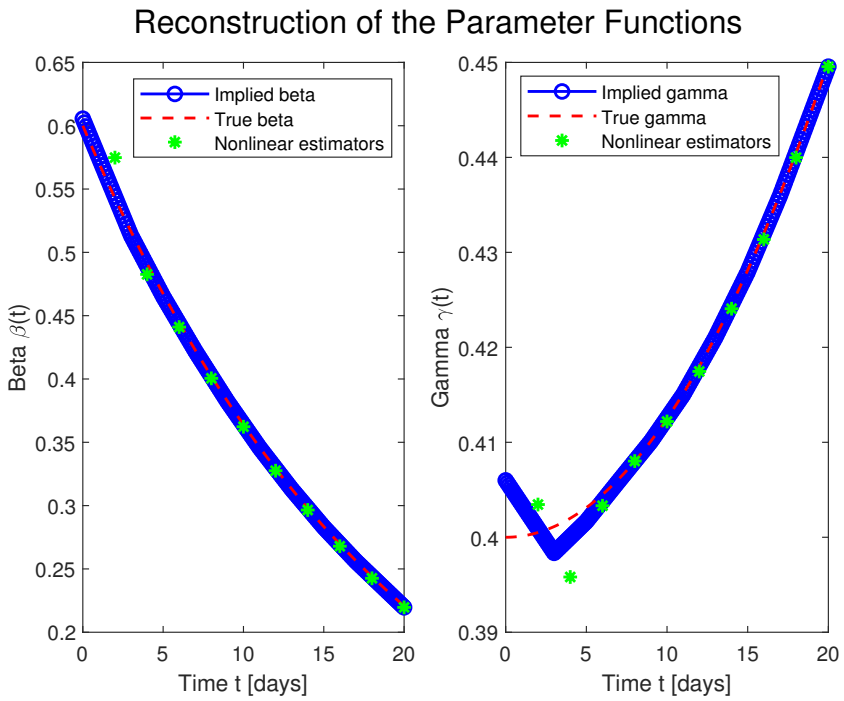

Figure 2. Recovered parameters $\beta(t)$ and $\gamma(t)$ with (12).

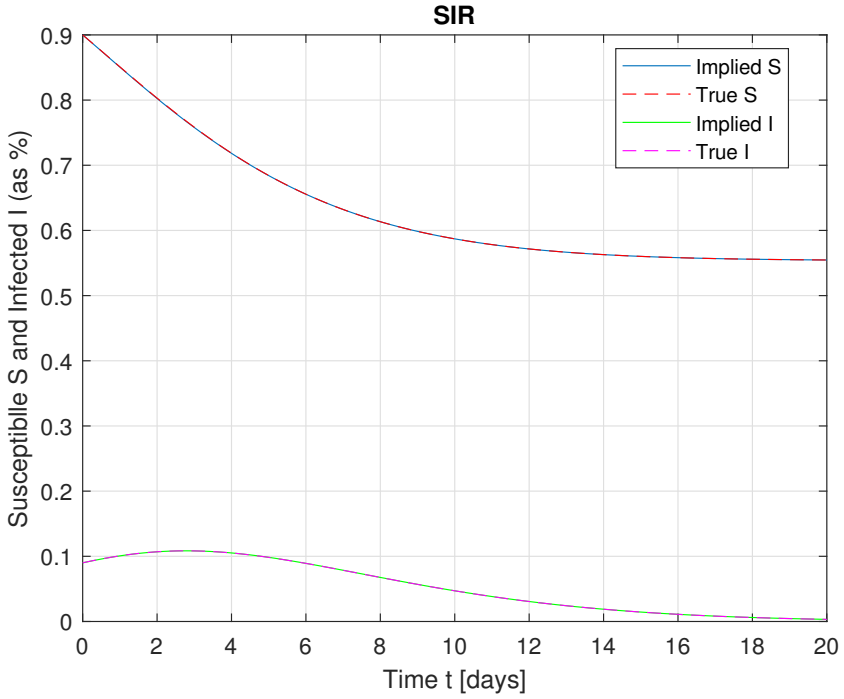

Figure 3. Recovered susceptible S and infected I population with (12).

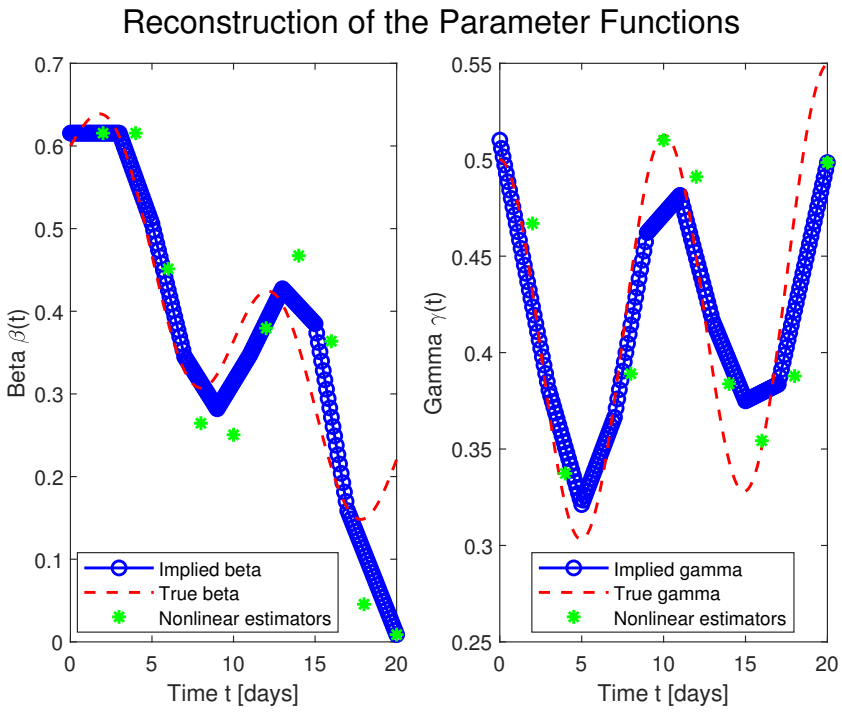

Figure 4. Recovered parameters $\beta(t)$ and $\gamma(t)$ with (14).

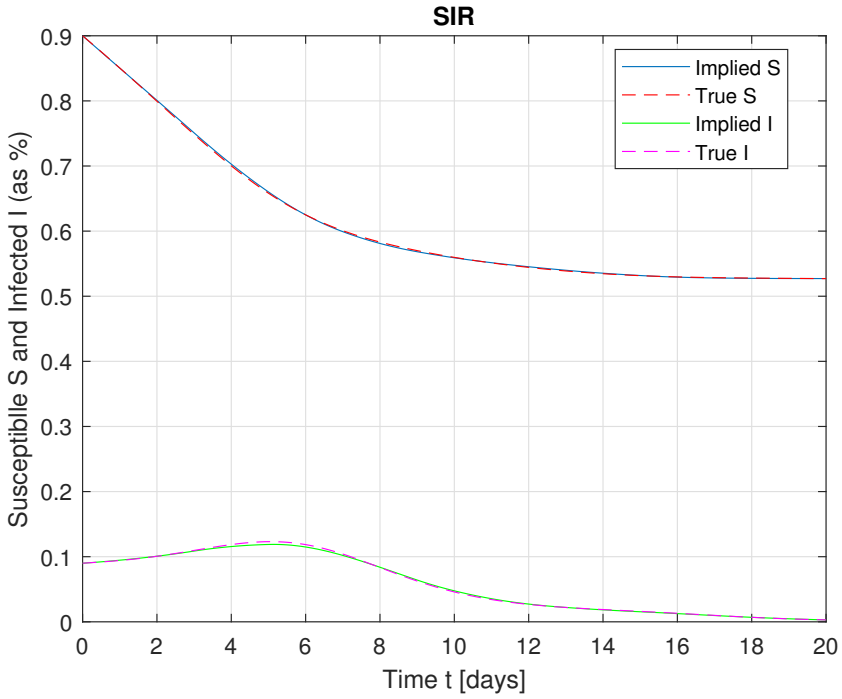

Figure 5. Recovered susceptible S and infected I population with (14).

A piecewise linear function cannot follow such a curve exactly, but the trend dynamics are recognized, and the residual norm of the solution is not much higher: $R\big(\beta(t), \gamma(t)\big) = 0.0412$.

7.2. Fractional-Order Derivative Model

Now, we continue the tests with the fractional model (2). It is solved by means of Algorithm 2. We use the same values for the initial condition, temporal steps and observations setting.

It is a well known "rule of thumb" that usually the optimal fractional derivative order is less than one but closer to one than to zero. So, now we conduct tests with $\alpha = 0.9$, while in Section 7.3, we show how to easily find the optimal order.

Firstly, we present the results with (12). Since they do not differ significantly with their integer-order counterparts, we plot them together in one Figure 6.

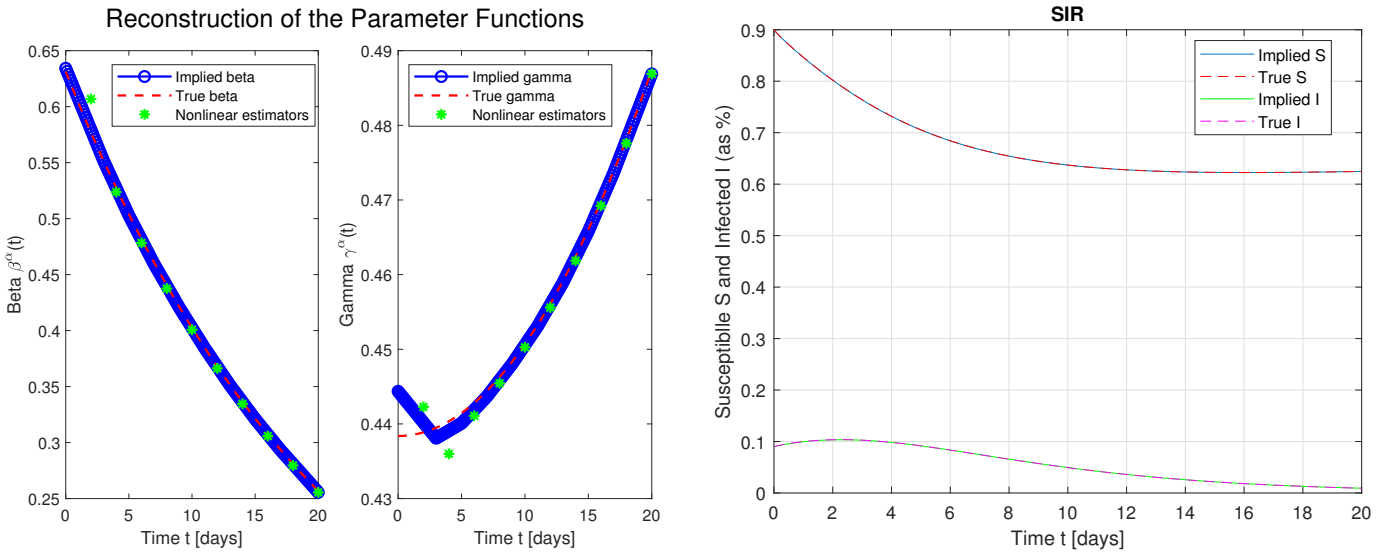

Figure 6. Recovered parameters $\beta^{\alpha}(t)$ and $\gamma^{\alpha}(t)$ with (12) (**left**); recovered susceptible S and infected I population with (12) (**right**).

Now, the residual norm is less than the integer-order case: $R\left(\beta^{\alpha}(t), \gamma^{\alpha}(t)\right) = 0.0027$. The implications are similar with the coefficients (14); see Figure 7.

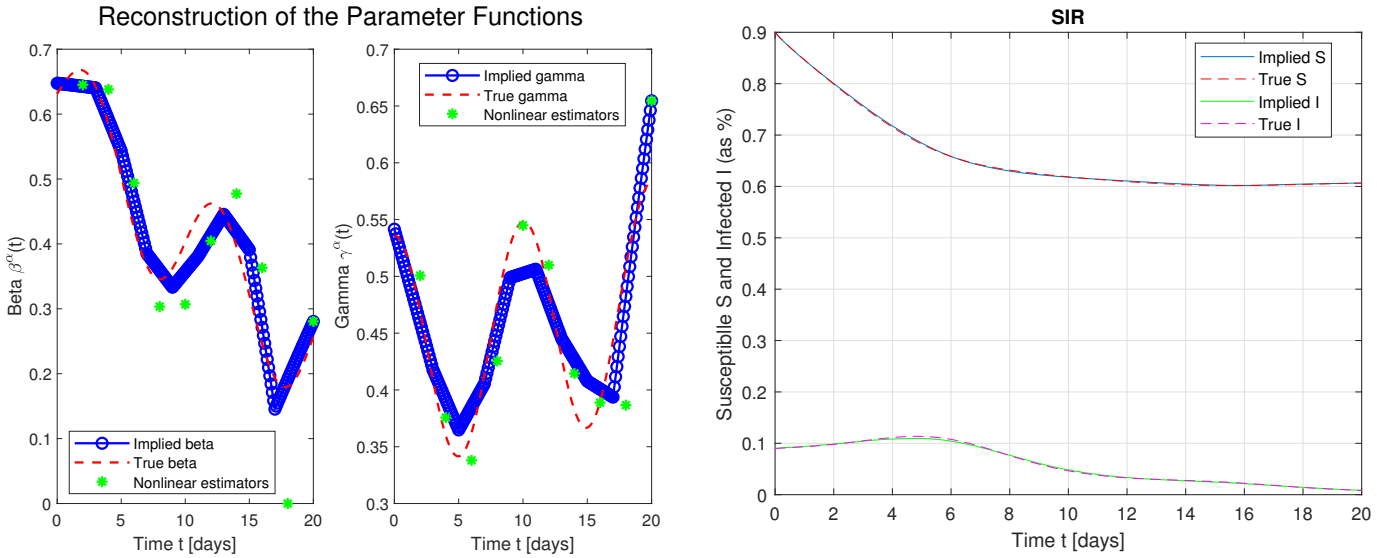

Figure 7. Recovered parameters $\beta^{\alpha}(t)$ and $\gamma^{\alpha}(t)$ with (14) (**left**); recovered susceptible S and infected I population with (14) (**right**).

Again, quite expectedly, the visual match of the coefficients (Figure 7, left) is better, and the residual norm is smaller: $R\left(\beta^{\alpha}(t), \gamma^{\alpha}(t)\right) = 0.0405$.

7.3. Real Data Fit

In this subsection, we consider the real-world data test with the official data for the Republic of Bulgaria [30]. The generalized SIR model is suitable for modeling the disease

dynamics in Bulgaria since the level of vaccination there is low. The data used are for 2022, since the tests (PCR and rapid antigen) are enough in number to conceptualize the epidemic situation in the country.

To obtain the infected population time series, we use the 'Active Cases' data. However, it is well known that actual cases are severely under-reported. To get closer to reality, we need to multiply the reported series with an escalation coefficient. Its exact value is unknown. The authors of [31] advise its default value is 3. In [32], it is stated it could be higher than 6. We chose a moderate value of 5. The recovered coefficients are weakly influenced by this choice, but the basic reproduction number, as a unitless quantity, is not influenced at all.

The removed time series is constructed by the sum of 'Recovered' and 'Deceased' data. Analogously, in order to fulfill property **P3** (susceptibles cannot grow in time), we need to multiply the removed series by the same escalation coefficient and eventually to compute $S(t) = 1 - I(t) - R(t)$.

The real data are very «rough», so we smoothen it with a simple moving average (SMA) filter with a period of 7 days (one week). Due to this transformation, we lose 6 time nodes, so to derive smooth data from 1 January 2022, we take a couple of earlier raw data elements (from 26 December 2021). We use the data available up to the moment of writing this paper, i.e., 12 October 2022.

The data are available for every day, and the main observations are equidistantly distributed on a weekly basis. The initial approximation of the parameters are as neutral as $\beta_0 = 0.5$ and $\gamma_0 = 0.5$.

To begin with, we calibrate the integer-order model (1), (3), (6). The result is plotted on Figures 8 and 9, while $\mathcal{R}_0$ is calculated through (4). The residual norm is $R\big(\beta(t), \gamma(t)\big) = 0.0416$.

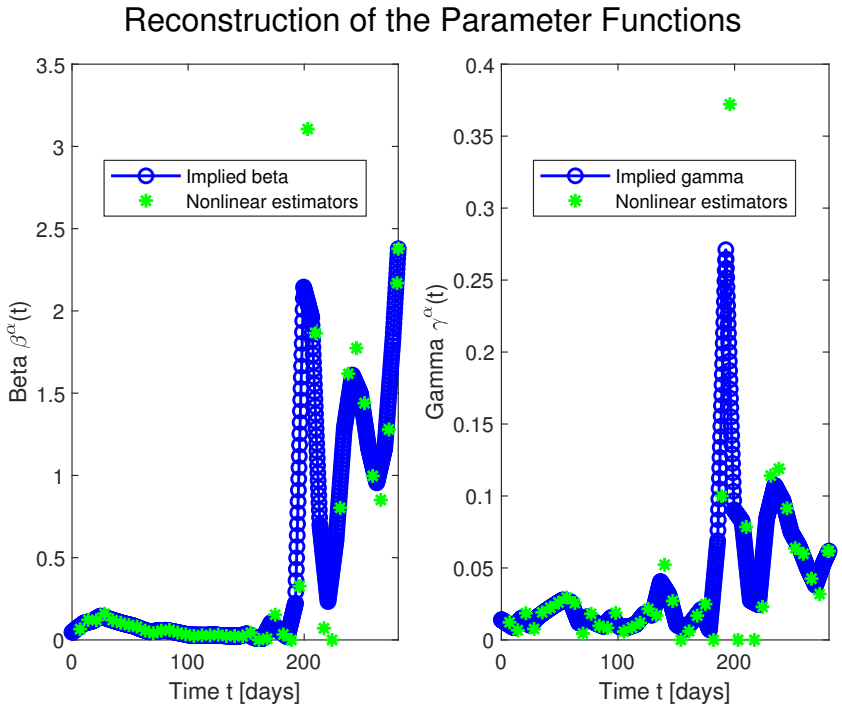

Figure 8. Recovered parameters $\beta(t)$ and $\gamma(t)$ for $\alpha = 1$.

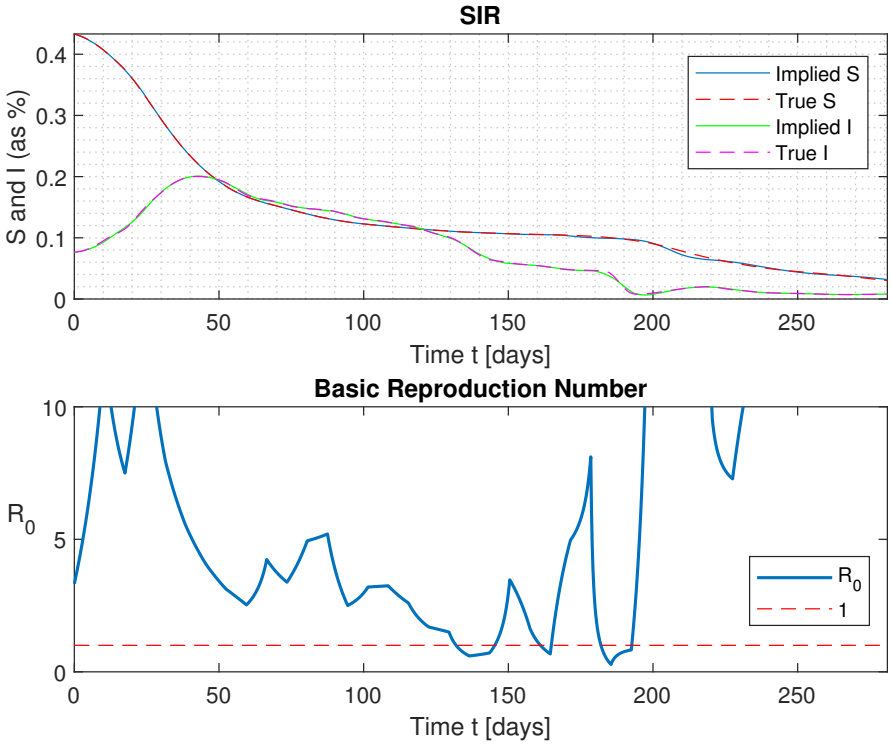

Figure 9. Recovered and observed susceptible S and infected I population (**top**) and the basic reproduction number $\mathcal{R}_0$ (**bottom**) for $\alpha = 1$.

At the end of 2021, Bulgaria entered the fifth wave [29], which reached its peak in the middle of February 2022 (Figure 9). For that period, the basic reproduction number is also high. With the weather getting warmer, the number of infected gradually drops until around the 200th day (second half of July), where the new wave commences. Then, both $\beta(t)$ and $\gamma(t)$ increase, expectedly, the transition rate is to a greater extent. So does $\mathcal{R}_0$. Only the absolute level of infected does not jump highly, but this is because most of the people have already contacted the virus and have gained natural immunity, thus being not susceptible.

The population of the Republic of Bulgaria is $N = 6{,}519{,}789$ [33]. The relative expenditures for medical treatment are $a =$USD 50 day^{-1} and the relative economic losses for reduced activity are $b =$ USD 500 day^{-1} (11). For the integer-order calibration, L =USD 16,646,280,321.61 for the year 2022 (up to 12 October). The first component of the losses, regarding the curing, is eight times more than the second component, concerning the economic reduction. This is normal since there were few and not long periods in 2022 when the nonessential businesses were closed.

Let us now continue with calibrating the fractional-order model (2). Usually, the fractional models give a better fit than their integer counterparts. What is more, the optimal fractional order is expected to be less than one but greater than a half. This observation is confirmed by the experiments. We conducted tests with different values of α, following a simple binary search over the residual norm (13). The results are presented in Table 1 and Figure 10.

All these findings suggest that the four significant digits in the optimal fractional order are $\alpha \approx 0.9437$.

Table 1. Residual norm for different α.

α	R
1	0.0415767359803674
0.95	0.0343187221232409
0.946875	0.0342537598193364
0.9453125	0.0342369859008066
0.94453125	0.0342327085301880
0.944140625	0.0342315962777517
0.9439453125	0.0342313804192775
0.943798828125	0.0342312496769189
0.94375	0.0342312372883962
0.94373779296875	0.0342312519248410
0.9437255859375	0.0342312347414336
0.943701171875	0.0342312483883185
0.94365234375	0.0342312415060524
0.9435546875	0.0342313292646742
0.943359375	0.0342315362284156
0.9375	0.0343261290485330
0.925	0.0351492607828226
0.9	0.0394191574626068

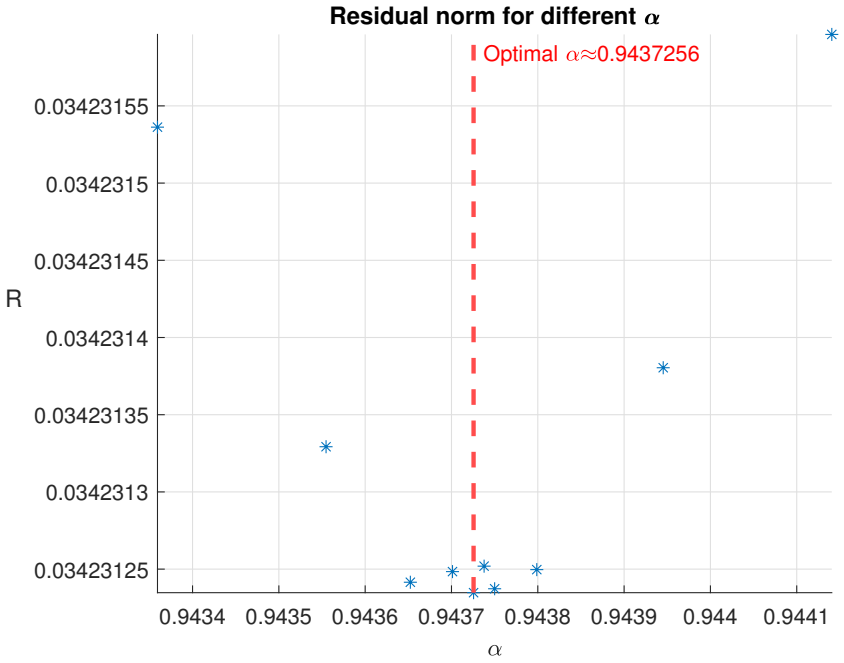

Figure 10. The residual norm (13) for different values of α.

The output from the calibration with $\alpha = 0.9437255859375$ is presented in Figures 11 and 12. Please note that the basic reproduction number is calculated via (5). The residual norm is less compared with the integer-order case: $R\left(\beta^{\alpha}(t), \gamma^{\alpha}(t)\right) = 0.0342$.

One might be tempted to find the optimal value of the fractional order via minimizing the functional

$$\min_{\alpha} \Phi(\alpha), \qquad \text{where} \qquad \Phi(\alpha) := R\left(\beta^{\alpha}(t), \gamma^{\alpha}(t)\right),$$

which is again the residual (13) of the fractional-order model calibration. This approach may be valid, but the functional has multiple local minima (Figure 10), thus a special minimization procedure must be applied with care.

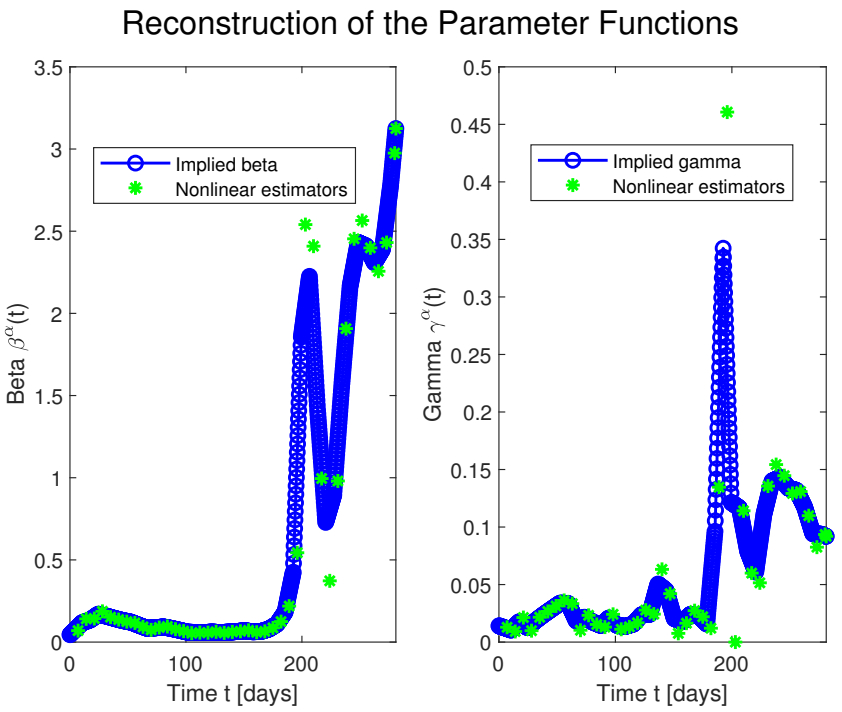

Figure 11. Recovered parameters $\beta^{\alpha}(t)$ and $\gamma^{\alpha}(t)$ for $\alpha = 0.9437255859375$.

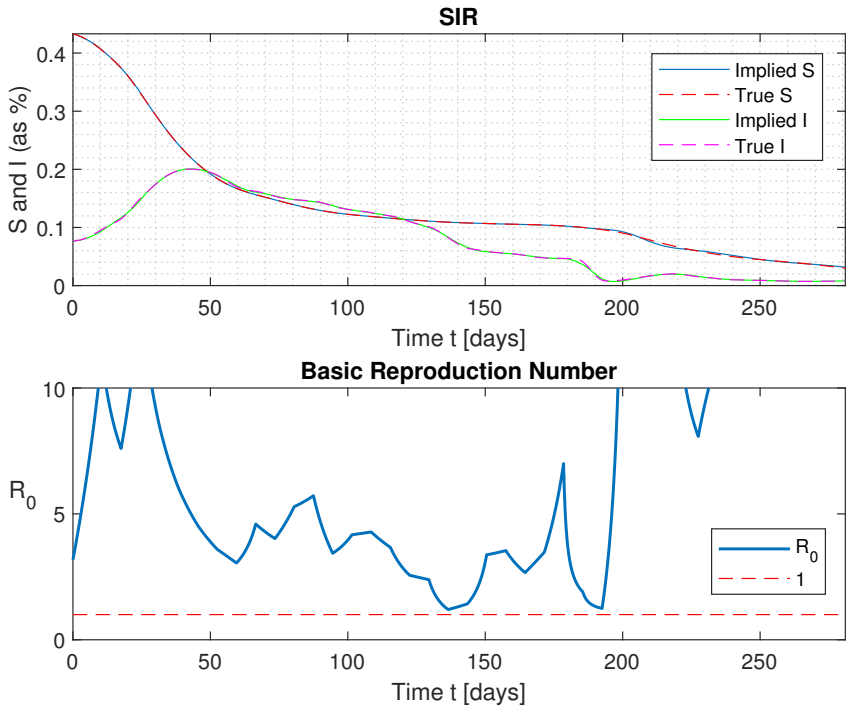

Figure 12. Recovered and observed susceptible S and infected I population (**top**) and the basic reproduction number $\mathcal{R}_0$ (**bottom**) for $\alpha = 0.9437255859375$.

Under the same assumptions, the epidermic impact is estimated to L = $USD13,203,180,389.91 for the year 2022. It is useful to mention that $\beta(t) := \beta^{\alpha}(t)$ in (11) for the fractional-order case. This is a bit less than the result from the integer-order estimation, but this will be considered as more reliable. Here, the first component of the losses is 13 times greater than the second component. Both estimates are higher than

the losses evaluated for the year 2021 in [29]. This is not surprising since in the latter no escalation coefficient was used.

Since the optimal α is close to one, the implied $\beta(t)$ and $\gamma(t)$ are very similar in the integer- and fractional-order cases (Figures 8 and 11). So are the basic reproduction numbers $\mathcal{R}_0$ (Figures 9 and 12). It could be easily observed that the moments when $\mathcal{R}_0$ becomes greater than one precede the 'waves' or the increases in the number of infected individuals. Since the beginning of September 2022, the Republic of Bulgaria has entered a plateau, which is not expected to break out in a wave since the number of susceptibles is already low.

8. Conclusions

This paper deals with a generalized SIR epidemic model. It is a compartment model with standard compartments into which a population is divided: the group S of individuals who are susceptible to the disease and can become infected, the group I of individuals who are infectious and are capable of infecting other individuals during encounter and the group R of removed individuals who either are deceased or gained life-long immunity at recovery and cannot get infected anymore. The latter assumption can be relaxed [5].

The considered model extends the basic one in two ways. Firstly, the dynamics parameters are modeled as functions of time instead of constants, which makes the model flexible to fit the data in a better way. It is a well-known fact that the transmission and recovery rate change due tho the change in policy and people's behavior. It is also known that the number of infected individuals today depends not only on its previous level but on the history of the infection, too. This phenomenon is captured by the usage of fractional-order derivatives, and this is the second enhancement of the classical model.

The study has also two aims. The first one is to propose a detailed algorithm for reconstruction of the time-dependent parameters. It is performed via a predictor–corrector approach, which is fast, robust and capable of processing real data. The second aim is to suggest a framework to evaluate the economic impact of the pandemic and the associated nonpharmaceutical interventions.

All these findings could be applied to other models. The basic homogeneous model can be extended to other compartments (SEIR, SEIS, MSIR, MSEIR, MSEIRS, etc.), vaccination, region, age and other heterogeneity of population, disease parameter heterogeneity and so on.

The results could be used for analysis of such possible interventions. The recovered values of the transition and recovering rates best evaluate the already undertaken measures and help local authorities to make the most adequate decisions when facing an upcoming wave. The economic losses assessment is beneficial when conducting simulations to choose the most suitable approach for fighting epidemics, while preserving both the people's health and the national budget.

However, the described approach is not limited to epidemiological modeling. The calibration of inverse problems arises everywhere, and they are more difficult to solve and often more important than their forward counterparts. The computational methods could be used in the fitting and analysis of any kind of dynamics system modeling natural phenomena and anthropogenic activities. The numerical algorithms, tested with real-world data, could be applied successfully to all areas of science.

Author Contributions: Conceptualization, S.G. and L.V.; methodology, S.G. and L.V.; software, S.G.; validation, S.G.; formal analysis, L.V.; investigation, S.G. and L.V.; resources, S.G. and L.V.; data curation, S.G.; writing—original draft preparation, S.G.; writing—review and editing, S.G. and L.V.; visualization, S.G.; supervision, L.V.; project administration, L.V.; funding acquisition, S.G. and L.V. All authors have read and agreed to the published version of the manuscript.

Funding: This research was funded by the Bulgarian National Science Fund under Young Scientists Project KP-06-M32/2–17.12.2019 "Advanced Stochastic and Deterministic Approaches for Large-Scale Problems of Computational Mathematics" and Scientific Research Fund of University of Ruse under FNSE-03.

Institutional Review Board Statement: Not applicable.

Informed Consent Statement: Not applicable.

Data Availability Statement: The data used for the study are freely available at [30].

Acknowledgments: The authors want to thank the Special Issue Organizers and the Mathematics Editors for waiving the APC. The authors are grateful to the anonymous referees for the useful suggestion and comments.

Conflicts of Interest: The authors declare no conflict of interest. The funders had no role in the design of the study; in the collection, analyses, or interpretation of data; in the writing of the manuscript; or in the decision to publish the results.

Abbreviations

The following abbreviations are used in this manuscript:

SARS-CoV-2	Severe Acute Respiratory Syndrome Coronavirus 2
(M)S(E)IR	(Passively immune by maternal antibodies-) Susceptible-(Exposed-) Infected-Removed
ODE	Ordinary Differential Equation(s)
AC	Absolutely continuous
GMF	Generalized mean value formula

References

1. Hethcote, H.W. The mathematics of infectious diseases. *SIAM Rev.* **2000**, *42*, 599–653. [CrossRef]
2. Kermack, W.O.; McKendrick, A.G. A contribution to the mathematical theory of epidemics. *Proc. R. Soc. Lond. Ser. A* **1927**, *115*, 700–721.
3. Hethcote, H.W. Three Basic Epidemilogical Models. In *Applied Mathematical Ecology*; Levin, S.A., Hallam, T.G., Gross, L.G., Eds.; Springer: Berlin/Heidelberg, Germany, 1989.
4. Munoz-Pacheco, J.M.; Posadas-Castillo, C.; Zambrano-Serrano, E. The Effect of a Non-Local Fractional Operator in an Asymmetrical Glucose-Insulin Regulatory System: Analysis, Synchronization and Electronic Implementation. *Symmetry* **2020**, *12*, 1395. [CrossRef]
5. Ehrhardt, M.; Gašper, J.; Kilianová, S. SIR-based mathematical modeling of infectious diseases withh vaccination and waning imunity. *J. Comput. Sci.* **2019**, *37*, 101027. [CrossRef]
6. Kumar, R.; Kumar, S. A new fractional modelling of Susceptible-Infected-Recovered equations with constant vaccination rate. *Nonlin. Eng.* **2014**, *3*, 11–19. [CrossRef]
7. Djenina, N.; Ouannas, A.; Batiha, I.M.; Grassi, G.; Oussaeif, T.-E.; Momani, S. A novel fractional-order discrete SIR model for predicting COVID-19 behavior. *Mathematics* **2022**, *10*, 2224. [CrossRef]
8. Naik, P.A. Global dynamics of a fractional-order SIR epidemic model with memory. *Int. J. Biomath.* **2020**, *13*, 2050071. [CrossRef]
9. Akossi, A.; Chowell-Puente, G.; Smirnova, A. Numerical study of discretization algorithms for stable estimation of disease parameters and epidemic forecasting. *Math. Biosci. Eng.* **2019**, *16*, 3674–3693. [CrossRef]
10. Ji, Q.; Zhao, X.; Ma, H.; Liu, Q.; Liu, Y.; Guan, Q. Estimation of COVID-19 transmission and advice on public health interventions. *Mathematics* **2021**, *9*, 2849.
11. Marinov, T.T.; Marinova, R.S. COVID-19 analysis using inverse problem for coefficient identification in SIR epidemic models. *Chaos Solitons Fractals X* **2020**, *5*, 100041. [CrossRef]
12. Marinov, T.T.; Marinova, R.S. Inverse problem for adaptive SIR model: Application to COVID–19 in Latin America. *Inf. Dis. Model.* **2022**, *7*, 134–148. [CrossRef] [PubMed]
13. Georgiev, S.; Vulkov, L. Coefficient identification for SEIR model and economic forecasting in the propagation of COVID-19. *Stud. Comput. Intell.* 2022, *in press*.
14. Georgiev, S.; Vulkov, L. Identification of COVID-19 dynamics and economic impact for a fractional SEIR model. *AIP Conf. Proc.* **2022**, *2505*, 080025.
15. Samuel, J.; Sinha, S. Optimal control in pandemics. *Phys. Rev. E.* **2021**, *103*, L010301. [CrossRef] [PubMed]
16. Brauer, F.; Castillo-Chavez, C.; Feng, Z. *Mathematical Models in Epidemiology*; Texts in Applied Mathematics; Springer: Berlin/Heidelberg, Germany, 2019; Volume 69.
17. Rida, S.Z.; Abdel Rady, A.S.; Arafa, A.A.M.; Khalil, M. Approximate analytical solution of the fractional epidemic model. *Int. J. Appl. Math. Res.* **2012**, *1*, 17–29. [CrossRef]
18. Love, E.R. Fractional derivatives of imaginary order. *J. Lond. Math. Soc.* **1971**, *3*, 241–259. [CrossRef]
19. Sardar, T.; Rana, S.; Bhattacharya, S.; Al-Khaled, K.; Chattopadhyay, J. A generic model for a single strain mosquito-transmitted disease with memory on the host and the vector. *Math. Biosci.* **2015**, *263*, 8–36. [CrossRef]

20. Chowell, G.; Brauer, F. The basic reproduction number of infectious diseases: Computation and estimation using compartmental epidemic models. In *Mathematical and Statistical Estimation Approaches in Epidemiology*; Chowell, G., Hyman, J.M., Bettencourt, L.M.A., Castillo-Chavez C., Eds.; Springer: Dordrecht, The Netherlands, 2009; pp. 1–30.
21. van den Driessche, P.; Watmough, J. Reproduction numbers and sub-threshold endemic equilibria for compartmental models of disease transmission. *Math. Biosci.* **2002**, *180*, 29–48. [CrossRef]
22. Diekmann, O.; Heesterbeek, J.A.P.; Metz, J.A.J. On the definition and the computation of the basic reproduction ratio R_0 in models for infectious diseases. *J. Math. Biol.* **1990**, *35*, 503–522.
23. Baleanu, D.; Diethelm, K.; Scalas, E.; Trujillo, J.J. *Fractional Calculus. Models and Numerical Methods*; World Scientific: Singapore, 2017.
24. Hundsdorfer, W.; Vermer, J. *Numerical Solution of Time-Dependent Advection-Diffusion-Reaction Equations*; Springer: Berlin/Heidelberg, Germany, 2003.
25. Lin, W. Global existence theory and chaos control of fractional differential equations. *J. Math. Anal. Appl.* **2007**, *332*, 709–726. [CrossRef]
26. Press, W.H.; Teukolsky, S.A.; Vetterling, W.T.; Flannery, B.P. *Numerical Recipes: The Art of Scientific Computing*, 3rd ed.; Cambridge University Press: Cambridge, UK, 2007.
27. Li, C.; Tao, C. On the fractional Adams method. *Comput. Math. Appl.* **2009**, *58*, 1573–1588. [CrossRef]
28. Kahalé, N. On the Economic Impact of Social Distancing Measures. 2020. Available online: http://dx.doi.org/10.2139/ssrn.3578415 (accessed on 13 October 2022).
29. Georgiev, S.; Vulkov, L. Coefficient identification in a SIS fractional-order modelling of economic losses in the propagation of COVID-19. *J. Comput. Sci.* 2022, *accepted*.
30. Coronavirus Statistics. 2022. Available online: https://coronavirus.bg/bg/statistika (accessed on 13 October 2022).
31. Kounchev, O.; Simeonov, G.; Kuncheva, Z. The TVBG-SEIR spline model for analysis of COVID-19 spread, and a tool for prediction scenarios. *arXiv* **2020**, arXiv:2004.11338v2.
32. Albani, V.; Loria, J.; Massad, E.; Zubelli, J. COVID-19 underreporting and its impact on vaccination strategies. *BMC Infect. Dis.* **2021**, *21*, 1111. [CrossRef] [PubMed]
33. Census 2021. 2022. Available online: https://census2021.bg (accessed on 13 October 2022).